Low-Temperature and Solution-Processed Amorphous WOX as Electron-Selective Layer for Perovskite Solar Cells

ARTICLE *in* JOURNAL OF PHYSICAL CHEMISTRY LETTERS · MARCH 2015

Impact Factor: 7.46 · DOI: 10.1021/acs.jpclett.5b00010

8 AUTHORS, INCLUDING:

Yantao Shi
Dalian University of Technology
52 PUBLICATIONS **454** CITATIONS
SEE PROFILE

Yu Li
Peking University
21 PUBLICATIONS **35** CITATIONS
SEE PROFILE

Shufeng Wang
Peking University
122 PUBLICATIONS **1,599** CITATIONS
SEE PROFILE

Tingli Ma
Dalian University of Technology
142 PUBLICATIONS **3,976** CITATIONS
SEE PROFILE

THE JOURNAL OF PHYSICAL CHEMISTRY Letters

Letter

pubs.acs.org/JPCL

Low-Temperature and Solution-Processed Amorphous WO_X as Electron-Selective Layer for Perovskite Solar Cells

Kai Wang,[†] Yantao Shi,*[,†] Qingshun Dong,[†] Yu Li,[§] Shufeng Wang,[§] Xufeng Yu,[†] Mengyao Wu,[†] and Tingli Ma*[,‡]

[†]State Key Laboratory of Fine Chemicals, School of Chemistry, Dalian University of Technology, #2 Linggong Road, Gaoxinyuan District, Dalian 116024, P. R. China

[‡]Graduate School of Life Science and Systems Engineering, Kyushu Institute of Technology, 2-4 Hibikino, Wakamatsu, Kitakyushu, Fukuoka 808-0196, Japan

[§]Department of Physics, Peking University, 209 Chengfu Road, Beijing 100871, P. R. China

Supporting Information

ABSTRACT: The electron-selective layer (ESL) is an indispensable component of perovskite solar cells (PSCs) and is responsible for the collection of photogenerated electrons. Preparing ESL at a low temperature is significant for future fabrication of flexible PSCs. In this work, solution-processed amorphous WO_x thin film was prepared facilely at low temperature and used as ESL in PSCs. Results indicated that a large quantity of nanocaves were observed in the WO_x thin film. In comparison with the conventional TiO_2 ESL, the WO_x ESL exhibited comparable light transmittance but higher electrical conductivity. Compared with the TiO_2-based PSCs, PSCs that use WO_x ESL exhibited comparable photoelectric conversion efficiency, larger short-circuit current density, but lower open-circuit voltage. Electrochemical characterization indicated that the unsatisfied open-circuit voltage and fill factor were caused by the inherent charge recombination. This study demonstrated that this material is an excellent candidate for ESL.

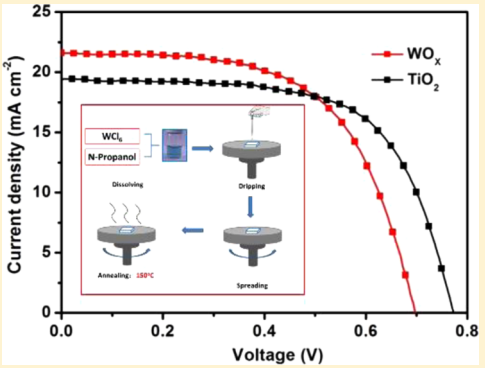

Third-generation photovoltaic devices that generate electricity from sunlight have been surging for several decades. With the aim of reducing the cost and achieving a high-efficiency, simplifying manufacturing process, many candidates, such as dye-sensitized solar cells (DSCs),[1,2] quantum dot solar cells (QDSCs),[3,4] and organic solar cells (OSCs),[5,6] have been developed and studied for years by scientists all over the world. Perovskite solar cells (PSCs) evolved from DSCs have become a rising star since their use as a photoabsorber for sensitized solar cells with photoelectric conversion efficiency (PCE) of 3.8% in 2009.[7] PSC performance has greatly progressed in recent years through revolutionary improvements in the device structure. Currently, Yang et al.[8] achieved the highest PCE of 19.3%. PSCs have diverse structures such as mesoscopic solar cells,[9−11] planar structure solar cells,[12−14] and so on. In general, PSCs consist of a transparent conductive substrate, an electron-selective layer (ESL), an optional mesoscopic layer, a perovskite layer, a hole transport material (HTM), and a metal cathode. Without no doubt, ESL is an electron collector that is indispensable in PSCs.

In general, high-temperature annealing is required to eliminate organic templates or additives in the fabrication of the conventional TiO_2 ESL.[15−17] However, annealing results in higher production cost and longer energy payback time. Thus, low-temperature preparation of ESL ought to be realized by improving the fabrication procedure or by developing novel ESL candidates for future production of flexible PSC devices based on a plastic substrate.[18−20] Several low-temperature approaches have been developed and reported to achieve comparable PCEs. In PSCs, TiO_2 is a commonly used ESL material. As we know, TiO_2 exhibits certain electrical conductivity only after the formation of nanocrystallites. Therefore, TiO_2 crystallite formation at a low temperature is the key point in the preparation of TiO_2 ESL. Grätzel et al. employed chemical bath deposition of $TiCl_4$ at 70 °C for 1 h for nanocrystalline formation, and PSCs based on this nanocrystalline exhibited an excellent PCE.[21] In addition, Snaith et al.[22] combined graphene and TiO_2 as ESL after preparing TiO_2 nanoparticles. The temperatures adopted were 150 °C or less, and a remarkable PCE was achieved. However, preparing low-temperature TiO_2 ESL is relatively complicated because TiO_2 crystallization is difficult. Although ZnO possesses high electron mobility (>200 $cm^2 \cdot V^{-1} \cdot s^{-1}$)[23,24] and can be also used as ESL in PSCs,[25] ZnO is chemically unstable and usually reacts with weak acids or weak bases. Thus, developing new technology or new functional materials is

Received: January 4, 2015
Accepted: February 2, 2015
Published: February 2, 2015

DOI: 10.1021/acs.jpclett.5b00010
J. Phys. Chem. Lett. 2015, 6, 755−759

urgently needed for the preparation of ESL at low temperature with simple processes.

Tungsten oxides (WO_x) are chemically stable semiconductors with wide bandgaps (2 to 3 eV)[26−30] and higher electron mobility (10−20 $cm^2 \cdot V^{-1} \cdot s^{-1}$).[31,32] These appealing properties enable efficient transportation of photogenerated electrons. Very recently, WO_x ESL was prepared for PSCs via high-temperature annealing, and a WO_x−TiO_2 core−shell nanostructure was applied to restrain charge recombination that occurs at the perovskite/WO_x interface.[33] So far, the use of low-temperature-processed WO_x as ESL in PSCs has never been reported. In this work, amorphous WO_x ESL was prepared for PSCs via solution route at low temperature. UV−visible (UV−vis) spectrum, X-ray powder diffraction (XRD), and scanning electron microscopy (SEM) were used to characterize the thin films in detail. The WO_x ESL exhibited excellent light transmittance and significantly higher electrical conductivity compared with conventional TiO_2. In addition, subsequent photo−luminescence decay indicated a faster kinetic process of charge transfer at the WO_x ESL/perovskite interface. These advantages enabled WO_x-based PSCs to provide higher short circuit current density (J_{SC}). Finally, a PCE of ∼8.99% was achieved by WO_x-based PSCs, which is comparable to that of for TiO_2-based PSCs (8.78%). It is believed that the photovoltaic performance of WO_x-based PSCs can be further improved through some strategies of suppressing the interface charge recombination.

Morphology of the WO_x ESL was characterized, and the top view SEM image is presented in Figure. 1a, from which a large

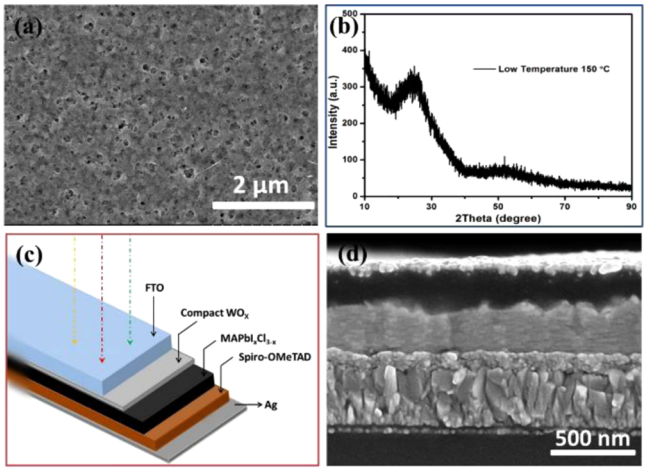

Figure 1. (a) Top view of the WO_x ESL. (b) X-ray diffraction patterns of low-temperature-processed WO_x at 150 °C. (c,d) Schematic structure and cross section SEM image of WO_x-based PSCs, respectively.

quantity of nanocaves were observed. These nanocaves were relatively shallow, and the FTO was completely covered and thus capable of retarding the charge recombination via preventing the direct contact with HTM effectively. These nanocaves provided an enlarged contact area between the ESL and perovskite, which are favorable for the collection of photogenerated electrons. Furthermore, Figure S2 in the Supporting Information shows that the WO_x ESL was very uniform, macroscopically. As is well known, crystallization of the ESL (in particular, for the commonly used TiO_2 compact thin film) has a significant effect on the charge collection. On the basis of the XRD characterization, our low-temperature and solution-processed WO_x ESL was almost amorphous (Figure 1b). However, the chemical composition of the low-temperature WO_x was roughly identical to the one processed at a high temperature of 500 °C (Figure S3 in the Supporting Information). Figure S4 in the Supporting Information shows the XPS analysis result of WO_x thin film. There were both W^{6+} and W^{5+} in this films, so we named this compound WO_x.[34−36] Figure 1c shows the configuration of the WO_x-based PSCs, in which the perovskite $CH3NH3PbI_xCl_{1-x}$ was sandwiched between the WO_x ESL-covered FTO glass and the Spiro-OMeTAD HTM. Figure 1d shows the cross-section of the WO_x-based PSCs. The thickness of the WO_x ESL was ∼150 nm, which is evidently thicker than the TiO_2 commonly used in previous reports. In this PSC device, the perovskite layer was ∼400 nm and relatively uniform over a large scale.

Photovoltaic performances of the PSCs based on WO_x or TiO_2 ESLs were measured under AM 1.5, 100 mW/cm^2 light illumination. J−V curves of these PSCs are illustrated in Figure 2, and the detailed parameters are summarized in Table 1. In

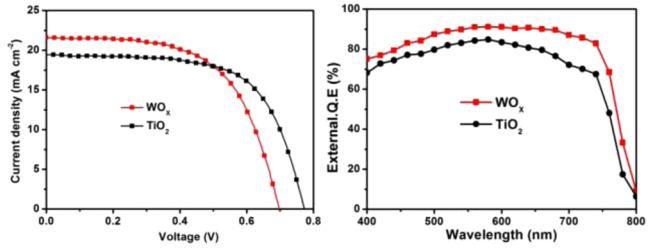

Figure 2. J−V curves and the IPCE of PSCs based on WO_x or TiO_2.

Table 1. Photovoltaic Parameters of PSCs based on WO_x or TiO_2.

ESL	V_{OC} (V)	J_{SC} (mA cm^{-2})	FF	efficiency (%)
TiO_2	0.75 ± 0.02	18.13 ± 1.33	0.64 ± 0.02	8.78 ± 0.79
WO_x	0.71 ± 0.03	21.77 ± 1.04	0.58 ± 0.02	8.99 ± 0.41

addition, the average data with error bars are illustrated in Figure 3. PSCs based on WO_x or TiO_2 ESLs showed comparable average PCEs of 8.99 and 8.78%, respectively.

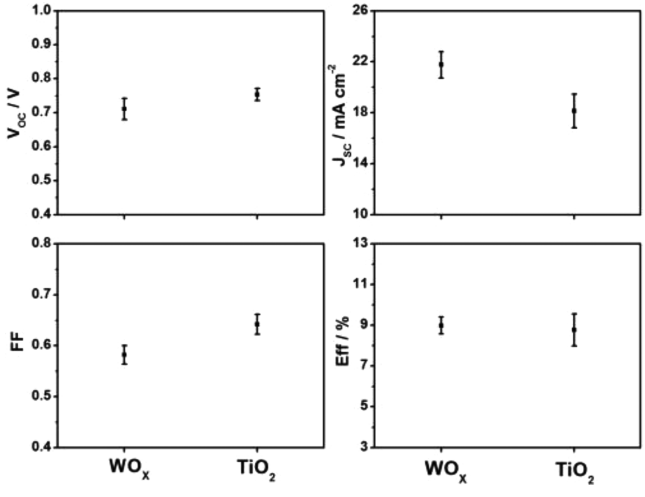

Figure 3. Effect of PSCs from WO_x or TiO_2 ESLs on photovoltaic parameters.

DOI: 10.1021/acs.jpclett.5b00010
J. Phys. Chem. Lett. 2015, 6, 755−759

Therefore, there was no significant difference in the photovoltaic performance between these two samples. Notably, our PSCs were prepared according to the published literature by Snaith, in which the PCE of TiO_2-based PSCs was reported to be 9.3%.[37] Therefore, the data we applied here for comparison were reliable. The average V_{OC}, J_{SC}, and FF of WO_x-based PSCs were 0.71 V, 21.77 mA cm^{-2}, and 0.58, respectively. The WO_x-based PSCs exhibited a higher J_{SC}, lower V_{OC}, and FF compared with the TiO_2-based samples. In addition, Figure 2b shows the IPCE of the device corresponding to the samples in Figure 2a. In detail, an impressive external quantum efficiency exceeding 70% can be observed across the whole visible region. Then, the IPCE intensity dropped drastically at a wavelength longer than 760 nm. The curve profile is similar to those reported in literature.[38] Indeed, the WO_x-based PSCs with higher J_{SC} also dominated in IPCE measurement. To interpret the inherent principle for the photovoltaic performance, we subsequently performed a series of characterizations.

For PSCs, several factors are crucial in determining the photovoltaic performance. The electrical conductivity of the ESL is extremely effective to PSCs. Therefore, linear sweep voltammetry (LSV) measurements were employed to analyze the electrical conductivity of the WO_x ESL. The symmetrical dummy cell was assembled by sandwiching HTM between two identical ESLs. Figure 4 shows that two straight lines passed

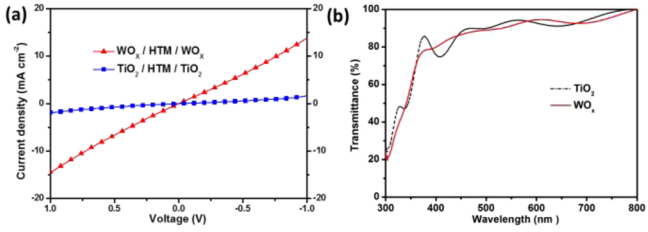

Figure 4. (a) Linear sweep voltammetry curves of TiO_2/HTM/TiO_2 and WO_x/HTM/WO_x. (b) UV−vis absorption spectra of $CH_3NH_3PbI_xCl_{3-x}/WO_x$ and $CH_3NH_3PbI_xCl_{3-x}/TiO_2$.

through the origin. WO_x evidently showed a higher current density, which indicated that WO_x ESL possessed higher electrical conductivity than TiO_2, favorable to the transport of electrons in ESL. This result was consistent with the fact that WO_x demonstrated higher electron mobility than TiO_2. As we know, the transmittance of the ESL could also affect the capture of incident light by a photoabsorber layer. As illustrated in Figure 4b, the transmittances of WO_x or TiO_2 ESLs both exceed 80% in the whole visible region, which favor the sufficient absorption of light by perovskite. Hence, the layer of WO_x exhibited excellent properties as an ESL for PSCs. Figure 5a shows the top view of $CH_3NH_3PbI_xCl_{3-x}/WO_x$ after deposition of perovskites. Similar with the TiO_2-based ESL (Figure S6), the ESL was almost fully coated by perovskite. However, the behaviors of the perovskite layers based on WO_x or TiO_2 during crystallization were fairly different. For the sample based on WO_x, three dominant diffraction peaks, designated to (110), (220), and (330) crystal planes of $CH_3NH_3PbI_xCl_{3-x}$, can be clearly observed, indicating oriented crystallization along ⟨110⟩.[12] By contrast, this phenomenon was not observed for the sample based on TiO_2. This result indicated that the ESL as a substrate had a certain effect on the crystallization of the subsequently deposited perovskite. Furthermore, the different crystallinities of perovskites could also lead to the variation in photoabsorptions. As shown in

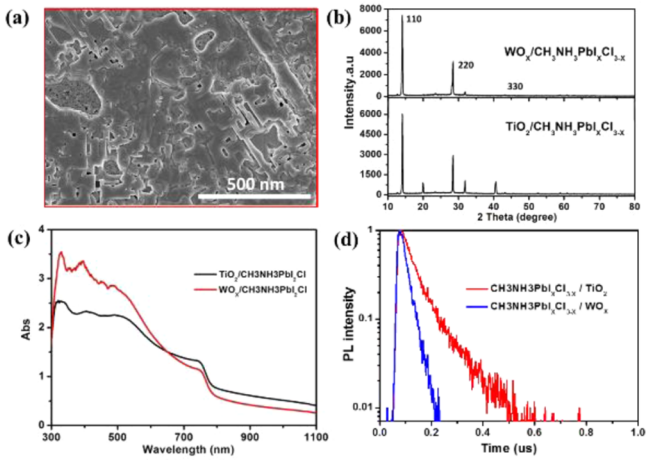

Figure 5. (a) Top view of the structure of $CH_3NH_3PbI_xCl_{3-x}/WO_x$. (b) X-ray diffractogram of $CH_3NH_3PbI_xCl_{3-x}/WO_x$ and $CH_3NH_3PbI_xCl_{3-x}/TiO_2$. (c) UV−vis absorption spectra of $CH_3NH_3PbI_xCl_{3-x}/WO_x$ and $CH_3NH_3PbI_xCl_{3-x}/TiO_2$. (d) Time-resolved PL decay measurements taken at 517 nm of $CH_3NH_3PbI_xCl_{3-x}/WO_x$ and $CH_3NH_3PbI_xCl_{3-x}/TiO_2$.

Figure 5c, a higher capability in light absorption was observed in the $CH_3NH_3PbI_xCl_{3-x}/WO_x$ device. For ESL in PSC, the capability in extracting photoinduced electrons from perovskite is also of great significance for the photovoltaic performance. Thus, we evaluated the kinetics of electron transfer at the ESL/perovskite interface by means of PL decay characterization. As illustrated in Figure 5d, the PL decay of the perovskites on WO_x ESL was much faster than that based on TiO_2, which suggests that the photoinduced electrons in perovskite could be more efficiently extracted by WO_x.[39] It was conjectured that for WO_x ESL the band structure (more negative conduction band level) and high carrier mobility could have contributed to the efficient electron extraction. All in all for WO_x ESL, the higher carrier mobility, good light transmittance and light absorption, and efficient charge extraction finally enabled WO_x-based PSCs to exhibit higher J_{SC}.

In this work, EIS characterization was conducted under dark conditions with a bias voltage of 0.6 V to determine the working principle and the mechanism of carrier transport and recombination. The Nyquist plot is composed of two irregular arcs, namely, a small arc at high frequency and a large arc at low frequency, as shown in Figure 6a.[40,41] The equivalent circuit is shown in Figure 6d. The first arc is usually attributed to the resistance (R_{hf}) of hole transporting in HTM and the charge transfer in the interface of HTM and perovskite (HTM/perovskite). The second arc is derived from the charge-transfer (ESL/perovskite) resistance R_{lf}. In addition, the value of the starting point at the real part of the Nyquist plot corresponds to the series resistance R_S.[42,43] Moreover, plots measured at other bias voltages (0, 0.3, and 0.8 V) displayed the same regularity with that using 0.6 V. As shown in Figure 6b, WO_x-based PSCs and TiO_2-based PSCs exhibited a similar resistance R_{hf}. As reported in the previous work, the charge-transport resistance in HTM was relevant to the HTM layer. In our experiment, the thicknesses of HTM in PSCs based on WO_x or TiO_2 were similar in the SEM image (Figure S5 in the Supporting Information). In addition, R_S is related to the resistance including that of external wires, the FTO substrate, and other additional contributions. Previous researchers had demonstrated that the ESL also had an effect on R_S.[40] Therefore, the R_S

DOI: 10.1021/acs.jpclett.5b00010
J. Phys. Chem. Lett. 2015, 6, 755−759

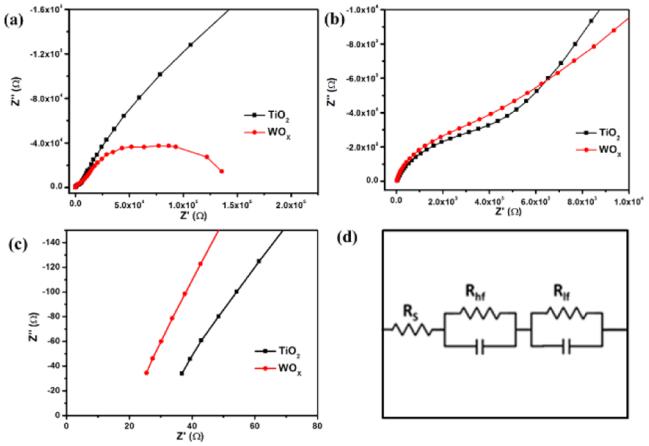

Figure 6. (a–c) Sequence of Nyquist plot of PSCs based on WO_x or TiO_2 in dark at 0.6 V. (d) Equivalent circuit.

values in our devices were ~10 Ω higher than that of TiO_2-based devices because of the higher carrier mobility of WO_x. We also observed that WO_x-based PSCs presented a much smaller resistance (R_{lf}) than that of TiO_2-based ones, as shown in Figure 6a. The span or diameter of the second arc reflects the resistance of charge recombination. Because of the low recombination rate, it was reasonable that TiO_2-based PSCs showed a higher V_{OC} than that of WO_x-based device.

In summary, WO_x ESL was easily prepared via a low-temperature solution-processing route for PSCs. WO_x ESL exhibited comparable light transmittance and relatively high electrical conductivity. Moreover, the WO_x ESLs had an effect on the oriented crystallization of perovskite, which is beneficial to the photoabsorption. Compared with TiO_2-based PSCs, a higher J_{SC} was obtained for the WO_x-based devices. Finally, an average PCE of 8.99% was achieved, which was comparable to the TiO_2 samples. It is believed that further advances in overall PCE can be achieved through suppressing the charge recombination. Moreover, the WO_x could also be used to prepare flexible PSCs because of the advantage of low-temperature preparation.

■ ASSOCIATED CONTENT

Supporting Information

Details of materials, device fabrication, and characterization. This material is available free of charge via the Internet at http://pubs.acs.org.

■ AUTHOR INFORMATION

Corresponding Authors

*T.M.: Tel/Fax: +86-411-84986237. E-mail: tinglima@life.kyutech.ac.jp.

*Y.S.: E-mail: shiyantao@dlut.edu.cn.

Notes

The authors declare no competing financial interest.

■ ACKNOWLEDGMENTS

This work is supported by the National Natural Science Foundation of China (Grant No. 51273032, 91333104) and the International Science & Technology Cooperation Program of China (Grant No. 2013DFA51000).

■ REFERENCES

(1) O'Regan, B.; Grätzel, M. a Low-Cost, High-Efficiency Solar Cell Based on Dye-Sensitized Colloidal TiO_2 Films. *Nature* **1991**, *353*, 737–740.

(2) Mathew, S.; Yella, A.; Gao, P.; Baker, R.; Curchod, B.; Astani, N.; Tavernelli, I. Dye-Sensitized Solar Cells with 13% Efficiency Achieved through the Molecular Engineering of Porphyrin Sensitizers. *Nat. Chem.* **2014**, *6*, 242–247.

(3) Lam, P.; Hatch, S.; Wu, J.; Tang, M.; Dorogan, V.; Mazur, Y.; Salamo, G.; Seeds, A.; Liu, H. Voltage Recovery in Charged InAs/GaAs Quantum Dot Solar Cells. *Nano Energy* **2014**, *6*, 159–166.

(4) Choi, H.; Kim, J.; Nahm, C.; Kim, C.; Nam, S.; Kang, J.; Lee, B.; Hwang, T.; Kang, S.; Choi, D.; Kim, Y.; Park, B. The Role of ZnO-Coating-Layer Thickness on the Recombination in CdS Quantum-Dot-Sensitized Solar Cells. *Nano Energy* **2013**, *2*, 1218–1224.

(5) Mao, L.; Chen, Q.; Li, Y.; Li, Y.; Cai, J.; Su, W.; Bai, S.; Jin, Y.; Ma, C.; Cui, Z.; Chen, L. Flexible Silver Grid/PEDOT:PSS Hybrid Electrodes for Large Area Inverted Polymer Solar Cells. *Nano Energy* **2014**, *10*, 259–267.

(6) Zimmermann, B.; Schleiermacher, H.; Niggemann, M.; Würfel, U. ITO-Free Flexible Inverted Organic Solar Cell Modules with High Fill Factor Prepared by Slot Die Coating. *Sol. Energy Mater. Solar Cells.* **2011**, *95*, 1587–1589.

(7) Kojima, A.; Teshima, K.; Shirai, Y.; Miyasaka, T. Organometal Halide Perovskites as Visible-Light Sensitizers for Photovoltaic Cells. *J. Am. Chem. Soc.* **2009**, *131*, 6050–6051.

(8) Zhou, H.; Chen, Q.; Li, G.; Luo, S.; Song, T.; Duan, H.; Hong, Z.; You, J.; Liu, Y.; Yang, Y. Interface Engineering of Highly Efficient Perovskite Solar Cells. *Science* **2014**, *345*, 542–546.

(9) Abrusci, A.; Stranks, S.; Docampo, P.; Yip, H.; Jen, A.; Snaith, H. High-Performance Perovskite-Polymer Hybrid Solar Cells via Electronic Coupling with Fullerene Monolayers. *Nano Lett.* **2013**, *13*, 3124–3128.

(10) Kim, H.; Lee, J.; Yantara, N.; Boix, P.; Kulkarni, S.; Mhaisalkar, S.; Gratzel, M.; Park, N. High Efficiency Solid-State Sensitized Solar Cell-Based on Submicrometer Rutile TiO_2 Nanorod and CH3NH3PbI3 Perovskite Sensitizer. *Nano Lett.* **2013**, *13*, 2412–2417.

(11) Burschka1, J.; Pellet, N.; Moon, S.; Humphry-Baker, R.; Gao, P.; Nazeeruddin, M.; Grätzel, M. Sequential Deposition As a Route to High-Performance Perovskite-Sensitized Solar Cells. *Nature* **2013**, *499*, 316–319.

(12) Liu, M.; Johnston, M.; Snaith, H. Efficient Planar Heterojunction Perovskite Solar Cells by Vapour Deposition. *Nature* **2013**, *501*, 395–398.

(13) Chen, Q.; Zhou, H.; Hong, Z.; Luo, S.; Wang, H.; Liu, Y.; Li, G.; Yang, Y. Planar Heterojunction Perovskite Solar Cells via Vapor-Assisted Solution Process. *J. Am. Chem. Soc.* **2014**, *136*, 622–625.

(14) Docampo, P.; Hanusch, F.; Stranks, S.; Döblinger, M.; Feckl, J.; Ehrensperger, M.; Minar, N.; Johnston, M.; Snaith, H.; Bein, T. Solution Deposition-Conversion for Planar Heterojunction Mixed Halide Perovskite Solar Cells. *Adv. Energy Mater.*, **2014**, *4*.

(15) Wu, Y.; Islam, A.; Yang, X.; Qin, C.; Liu, J.; Zhang, K.; Peng, W.; Han, L. Retarding the Crystallization of PbI_2 for Highly Reproducible Planar-Structured Perovskite Solar Cells via Sequential Deposition. *Energy Environ. Sci.* **2014**, *7*, 2934–2938.

(16) Eperona, G.; Stranksa, S.; Menelaou, C.; Johnstona, M.; Herza, L.; Snaith, H. Formamidinium Lead Trihalide: A Broadly Tunable Perovskite for Efficient Planar Heterojunction Solar Cells. *Energy Environ. Sci.* **2014**, *7*, 982–988.

(17) Ryu, S.; Noh, J.; Jeon, N.; Kim, Y.; Yang, W.; Seo, J.; Seok, S. Voltage Output of Efficient Perovskite Solar Cells with High Open-Circuit Voltage and Fill Factor. *Energy Environ. Sci.* **2014**, *7*, 2614–2618.

(18) Roldán-Carmona, C.; Malinkiewicz, O.; Soriano, A.; Espallargas, G.; Garcia, A.; Reinecke, P.; Kroyer, T.; Dar, M.; Nazeeruddin, M.; Bolink, H. Flexible High Efficiency Perovskite Solar Cells. *Energy Environ. Sci.* **2014**, *7*, 994–997.

(19) Chiang, Y.; Jeng, J.; Lee, M.; Peng, S.; Chen, P.; Guo, T.; Wen, T.; Hsu, Y.; Hsu, C. High Voltage and Efficient Bilayer Heterojunction

DOI: 10.1021/acs.jpclett.5b00010
J. Phys. Chem. Lett. 2015, 6, 755–759

Solar Cells Based on an Organic−inorganic Hybrid Perovskite Absorber with a Low-Cost Flexible Substrate. *Phys. Chem. Chem. Phys.* **2014**, *16*, 6033−6040.
(20) Kumar, M.; Yantara, N.; Dharani, S.; Grätzel, M.; Mhaisalkar, S.; Boix, P.; Mathews, N. Flexible, Low-Temperature, Solution Processed ZnO-Based Perovskite Solid State Solar Cells. *Chem. Commun.* **2013**, *49*, 11089−11091.
(21) Yella, A.; Heiniger, L.; Gao, P.; Nazeeruddin, M.; Grätzel, M. Nanocrystalline Rutile Electron Extraction Layer Enables Low-Temperature Solution Processed Perovskite Photovoltaics with 13.7% Efficiency. *Nano Lett.* **2014**, *14*, 2591−2596.
(22) Wang, J.; Ball, J.; Barea, E.; Alexander-Webber, A.; Huang, J.; Saliba, M.; Mora-Sero, I.; Bisquert, J.; Snaith, H. Low-Temperature Processed Electron Collection Layers of Graphene/TiO_2 Nanocomposites in Thin Film Perovskite Solar Cells. *Nano Lett.* **2014**, *14*, 724−730.
(23) Zhang, Q.; Dandeneau, C.; Zhou, X.; Cao, G. ZnO Nanostructures for Dye-Sensitized Solar Cells. *Adv. Mater.* **2009**, *21*, 4087.
(24) Shi, Y.; Wang, K.; Du, Y.; Zhang, H.; Gu, J.; Zhu, C.; Wang, L.; Guo, W.; Hagfeldt, A.; Wang, N.; Ma, T. Solid-State Synthesis of ZnO Nanostructures for Quasi-Solid Dye-Sensitized Solar Cells with High Efficiencies up to 6.46%. *Adv. Mater.* **2013**, *25*, 4413−4419.
(25) Liu, D.; Kelly, T. Perovskite Solar Cells with a Planar Heterojunction Structure Prepared Using Room-Temperature Solution Processing Techniques. *Nat. Photonics* **2014**, *8*, 133−138.
(26) Wang, F.; Valentin, C.; Pacchioni, G. Rational Band Gap Engineering of WO_3 Photocatalyst for Visible Light Water Splitting. *ChemCatChem.* **2012**, *4*, 476−478.
(27) Ottaviano, L.; Lozzi, L.; Passacantando, M.; Santucci, S. On the Spatially Resolved Electronic Structure of Polycrystalline WO_3 Films Investigated with Scanning Tunneling Spectroscopy. *Surf. Sci.* **2001**, *475*, 73−82.
(28) Dixon, R.; Williams, J.; Morris, D.; Rebane, J.; Jones, F.; Egdell, R.; Downes, S. Electronic States at Oxygen Deficient WO_3 (001) Surfaces: A Study by Resonant Photoemission. *Surf. Sci.* **1998**, *399*, 199−211.
(29) Washizu, E.; Yamamoto, A.; Abe, Y.; Kawamura, M.; Sasaki, K. Optical and Electrochromic Properties of RF Reactively Sputtered WO_3 Films. *Solid State Ionics* **2003**, *165*, 175−180.
(30) Weinhardt, L.; Blum, M.; Bar, M.; Heske, C.; Cole, B.; Marsen, B.; Miller, E. Electronic Surface Level Positions of WO3 Thin Films for Photoelectrochemical Hydrogen Production. *J. Phys. Chem. C* **2008**, *112*, 3078−3082.
(31) Berak, J.; Sienko, M. Effect of Oxygen-Deficiency on Electrical Transport Properties of Tungsten Trioxide Crystals. *J. Solid State Chem.* **1970**, *2*, 109−133.
(32) Gillet, M.; Aguir, K.; Lemire, C.; Gillet, E.; Schierbaum, K. The Structure and Electrical Conductivity of Vacuum-Annealed WO_3 Thin Films. *Thin Solid Films* **2004**, *467*, 239−246.
(33) Mahmood, K.; Swain, B.; Kirmania, A.; Amassian, A. Highly Efficient Perovskite Solar Cells Based on a Nanostructured WO_3−TiO_2 Core−Shell Electron Transporting Material. *J. Mater. Chem. A* **2014**, DOI: 10.1039/C4TA04883K.
(34) Guo, C.; Yin, S.; Yan, M.; Kobayashi, M.; Kakihana, M.; Sato, T. Morphology-Controlled Synthesis of $W_{18}O_{49}$ Nanostructures and Their Near-Infrared Absorption Properties. *Inorg. Chem.* **2012**, *51*, 4763−4771.
(35) Zhou, H.; Shi, Y.; Dong, Q.; Lin, J.; Wang, A.; Ma, T. Surface Oxygen Vacancy-Dependent Electrocatalytic Activity of $W_{18}O_{49}$ Nanowires. *J. Phys. Chem. C* **2014**, *118*, 20100−20106.
(36) Wang, X.; Jang, Y.; Yang, N.; Yuan, L.; Pang, S. XPS and XRD Study of the Electrochromic Mechanism of WO_X Films. *Surf. Coat. Technol.* **1998**, *99*, 82−86.
(37) Eperon, G.; Burlakov, V.; Docampo, P.; Goriely, A.; Snaith, H. Morphological Control for High Performance, Solution-Processed Planar Heterojunction Perovskite Solar Cells. *Adv. Funct Mater.* **2014**, *24*, 151−157.
(38) Lee, M.; Teuscher, J.; Miyasaka, T.; Murakami, T.; Snaith, H. Efficient Hybrid Solar Cells Based on Meso-Superstructured Organometal Halide Perovskites. *Science* **2012**, *338*, 643−647.
(39) Stranks, S.; Eperon, G.; Grancini, G.; Menelaou, C.; Alcocer, M.; Leijtens, T.; Herz, L.; Petrozza, A.; Snaith, H. Electron-Hole Diffusion Lengths Exceeding 1 Micrometer in an Organometal Trihalide Perovskite Absorber. *Science* **2013**, *342*, 341−344.
(40) Gonzalez-Pedro, V.; Juarez-Perez, E.; Arsyad, W.; Barea, E.; Fabregat-Santiago, F.; Mora-Sero, I.; Bisquert, J. General Working Principles of CH3NH3PbX3 Perovskite Solar Cells. *Nano Lett.* **2014**, *14*, 888−893.
(41) Juarez-Perez, E.; Wuβler, M.; Fabregat-Santiago, F.; Lakus-Wollny, K.; Mankel, E.; Mayer, T.; Jaegermann, W.; Mora-Sero, I. Role of the Selective Contacts in the Performance of Lead Halide Perovskite Solar Cells. *J. Phys. Chem. Lett.* **2014**, *5*, 680−685.
(42) Shi, Y.; Zhao, C.; Wei, H.; Guo, J.; Liang, S.; Wang, A.; Zhang, T.; Liu, J.; Ma, T. Single Atom Catalysis in Mesoporous Photovoltaics: The Principle of Utility Maximization. *Adv. Mater.* **2014**, *26* (48), 8147−8153.
(43) Edri, E.; Kirmayer, S.; Mukhopadhyay, S.; Gartsman, K.; Hodes, G.; Cahen, D. Elucidating the Charge Carrier Separation and Working Mechanism of $CH_3NH_3PbI_{3-x}Cl_x$ Perovskite Solar Cells. *Nat. Commun.* **2014**, *5*, 3461.

DOI: 10.1021/acs.jpclett.5b00010
J. Phys. Chem. Lett. 2015, 6, 755−759